RSC Advances

PAPER

View Article Online
View Journal | View Issue

Cite this: *RSC Adv.*, 2020, **10**, 34215

Rapid synthesis of cesium lead halide perovskite nanocrystals by L-lysine assisted solid-phase reaction at room temperature†

Yi-Lin Hu, Qiu-Lin Wen, Zheng-Fen Pu, An-Yong Liu, Jun Wang, Jian Ling,* Xiao-Guang Xie and Qiu-E. Cao*

Received 4th September 2020
Accepted 8th September 2020

DOI: 10.1039/d0ra07589b

rsc.li/rsc-advances

Nowadays, there are many ways to obtain cesium lead halide perovskite nanocrystals. In addition to the synthesis methods carried out in solution, the solid-phase synthesis was reported involving grinding and milling. In this paper, we synthesized luminescent $CsPbBr_3/Cs_4PbBr_6$ perovskite nanocrystals (PNCs) by three solid-phase synthesis methods (grinding, knocking, stirring) using L-lysine as a ligand. This is the first attempt to use an amino acid for assisting the solid phase synthesis of perovskite and to study the difference in the products obtained by the three solid phase synthesis methods. The results show that the productivity of the solid-phase synthesis methods can be greatly improved by adding L-lysine and the perovskites obtained by the methods are more resistant to water due to the addition of L-lysine. The simplicity of the synthesis process expanded the use of solid-phase synthesis to obtain more perovskites and provided potential applications of perovskite in analytical detection and sensing in aqueous solution.

1. Introduction

Lead-halide perovskite semiconductors are emerging materials that have many applications in photovoltaic cells,[1–10] solid-state lasers,[11–14] light-emitting diodes,[15] photodetectors,[16–19] and solar fuel production[20] due to their remarkable photoelectric effects. The synthesis of all-inorganic cesium lead halide perovskite can be traced back to 1893 when Wells and his collaborators showed that crystals of $CsPbX_3$ (X = Cl, Br or I) and Cs_4PbX_6 (X = Cl or Br) could be prepared from aqueous solutions.[21] In the field of synthesis of all-inorganic lead-halide perovskites, it is worth mentioning that Kovalenko and colleagues have developed a widely used synthetic route called the heat injection process.[22] Thereafter, the shape, dimensions and crystal phase of $CsPbX_3$ perovskite nanocrystals (PNCs) were designed by learning from the experience of classical cadmium chalcogenide nanocrystal synthesis.[23–26] In the synthesis of solution-based colloidal nanocrystals, the key is to obtain nanocrystals with green emission by solvent-induced reprecipitation using a capped ligand. The role of these ligands is to provide self-terminating of the crystallization, resulting in the formation of discrete nanoparticles in solution.[27] The termination of crystal growth by surface ligands is an important component of its nucleation and growth process, so the use of ligands affects material stability and photoluminescence quantum yield.[28]

Compared with the homogeneous synthesis in solution, the mechanochemical synthesis route is easy to implement, sustainable and energy-efficient. The greatest potential lies in the possibility of promoting a solid chemical reaction, and any reactant will become any product at room temperature because the reaction is triggered by mechanical stress rather than heat to overcome all thermodynamic reaction barriers.[29,30] One of the main advantages of mechanochemical synthesis is that no solvent is required. This is very important in the development of green chemistry because solvents usually represent large amounts of waste. In addition, many of them are harmful to human health and the environment. However, it is often difficult to stabilize the perovskite from the initial reactant powder mixture consisting of micron sized particles in a direct and rapid solid-phase synthesis.[31] Several studies have shown that the mechanical stress generated by ball impact can alter the reactant powder and reduce the calcination temperature and processing time.[32,33] In the mechanochemical synthesis of cesium lead-halide perovskites, grinding or ball milling is commonly used.[34,35] In addition to directly grinding cesium bromide and lead bromide in a vacuum drying oven,[36] large-scale synthesis of halogenated perovskite lead colloidal quantum dots in grinding can be achieved by direct wet grinding of the precursor.[37]

In this work, it is the first time to use amino acids as an assistant to directly solid-phase synthesizes all-inorganic cesium lead perovskites nanocrystals (PNCs) with bright luminescence. So far, the method of directly assisting the synthesis

Functional Molecules Analysis and Biotransformation Key Laboratory of Universities in Yunnan Province, National Demonstration Center for Experimental Chemistry and Chemical Engineering Education, School of Chemical Science and Engineering, Yunnan University, Kunming 650091, China. E-mail: lingjian@ynu.edu.cn; qecao@ynu.edu.cn; Fax: +86-871-65033679; Tel: +86-871-65033719

† Electronic supplementary information (ESI) available. See DOI: 10.1039/d0ra07589b

of luminescent PNCs by amino acids still requires the participation of organic solvents.[28] Under the premise of discarding both the vacuum grinding environment[31,35] and the organic solvent to obtain green luminescent nanoparticles, the method greatly simplifies the synthesis step and further realizes green chemistry in the field of perovskite synthesis. Furthermore, we studied three different types of solid-phase synthesis methods: grinding by mortar and pestle (grinding synthesis), knocking by magnetic stirrer bar (knocking synthesis) and stirring by vortex mixer (stirring synthesis). The difference among the three synthesis methods is the magnitude of force on mixing and dispersion of the mixing. The contact force of grinding synthesis is the largest, but the raw materials cannot well mixed. The knocking synthesis is moderate, and the stirring synthesis is just on the opposite. The results indicated that through the addition of L-lysine (Lys), after only 2 minutes of grinding, perovskite crystal formed, and great luminescence can be seen under UV light illumination. We also found that the solid-phased reaction by the stirring synthesis has advantages of simple operation steps and short synthesis time over other two solid-phase reactions (grinding and knocking synthesis). This study indicated that the top–down reaction of the perovskite nanostructure can be achieved by a simple solid phase reaction without long-time grinding.[34,36]

2. Experimental section

2.1 Materials and instruments

Lead(II) bromide (99%), cesium bromide (99.9%) and L-lysine (97%) were purchased from Adamas-beta. All chemicals were used as received without further purification. Ultrapure (UP) water (18.25 MΩ) was used throughout the experiments. The photoluminescence properties were measured using a F-7000 fluorescence spectrophotometer (Hitachi, Tokyo, Japan). FT-IR spectra were measured using a Nicolet iS10 Fourier Transform Infrared Spectrometer (American Thermo Fisher Scientific). The X-ray photoelectron spectroscopy (XPS) data were collected on a K-Alpha+ X-ray photoelectron spectrometer (Thermo Fisher Scientific). The luminescence photos of Lys-PNCs were captured in a ZF-1 ultraviolet analyzer under 365 nm of illumination. Transmission electron microscope (TEM) images were taken on JEM 2100 high-resolution transmission electron microscope (Hitachi, Ltd, Japan.) and FEI Tecnai G2 F20 (American FEI). The solid-phase reaction instruments are QL-901 vortex mixer (Haimen Bell Labs Instrument Co., Ltd., Haimen, China) and IKA RCT basic heating magnetic stirrer (IKA (Guangzhou) Instrument Equipment Co., Ltd.). X-ray diffraction (XRD) measurements were carried out using an Ultima IV diffractometer with monochromatized Cu Kα radiation at 40 kV and 40 mA and were recorded. The Photoluminescence lifetime (PLLT) properties were obtained by Fluorolog-3 spectrofluorometer (Horiba, USA).

2.2 Solid-phase synthesis of Lys-PNC by grinding, knocking and stirring

The solid-phase synthesis methods (grinding, knocking and stirring synthesis) were carried by the following instrument: (1) the grinding was carried out by mortar and pestle. The CsBr (0.2 mmol), L-Lysine (0.04 mmol) and $PbBr_2$ (0.2 mmol) were taken in the mortar to ensure that the ratio of the three substances was 1 : 0.2 : 1, and after 5 min of grinding, a perovskite solid with green photoluminescence emission can be obtained. (2) The knocking was implemented by a magnetic stirrer bar. The CsBr (0.2 mmol), L-lysine (0.04 mmol) and $PbBr_2$ (0.2 mmol) were taken in a 1.5 mL centrifuge tube to ensure that the ratio of the three substances was 1 : 0.2 : 1. The small magnetic stirrer bar (5 mm × 10 mm) were dropped into a 1.5 mL centrifuge tube, and the mixture was stirred for half an hour (700 rpm) to obtain a product with strong green photoluminescence. (3) The stirring was carried out by a vortex mixer. The CsBr (0.2 mmol), L-lysine (0.04 mmol) and $PbBr_2$ (0.2 mmol) were taken in a 1.5 mL centrifuge tube to ensure that the ratio of the three substances was 1 : 0.2 : 1, and the centrifuge tube was fastened

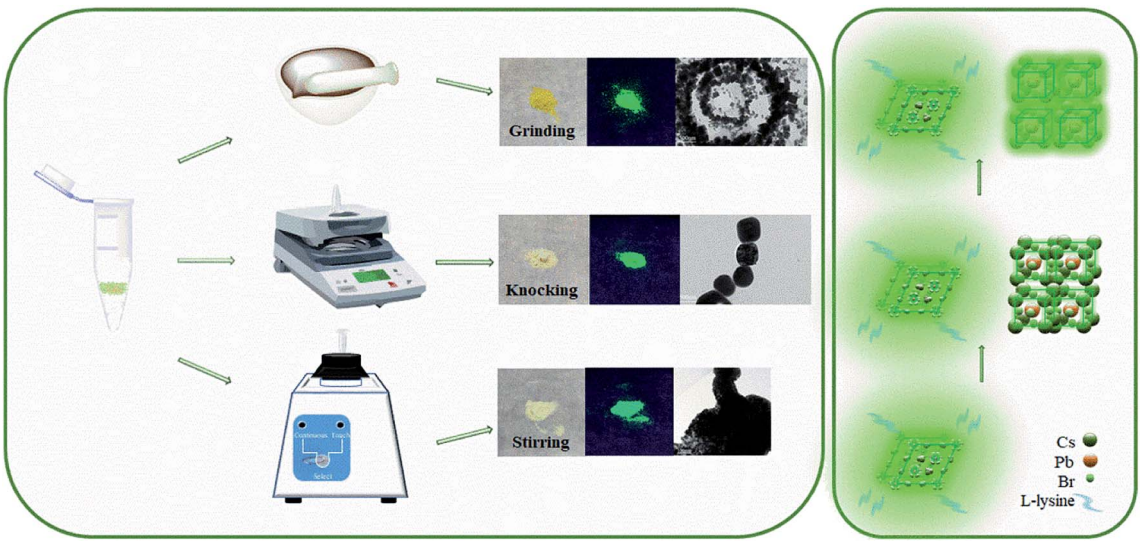

Fig. 1 Three solid-phase synthesis methods and schematic diagrams of the effects of L-lysine on Lys-PNCs.

on a vortex mixer (3000 rpm). After stirring for 20 min, it was taken off and left in the dark for 30 min to obtain a perovskite solid with green photoluminescence emission. The products obtained by the above three solid phase synthesis are all purified with ethanol.

2.3 Water assisted grinding synthesis of Lys-PNC

The CsBr (0.2 mmol), L-Lysine (0.2 mmol) and $PbBr_2$ (0.2 mmol) were added to the mortar in turn (to ensure that the ratio of the three substances was 1 : 1 : 1.1, slightly excess $PbBr_2$), and grinding was carried out for 2 min to obtain a pale-yellow viscosity blocky solid. Then, 1.0 mL of UP water was added in the mortar and continued the grinding, and the turbid liquid in the mortar was pale-yellow. The turbid liquid was applied to a glass slide and air-dried naturally, and the remaining white powder was a strong green photoluminescence Lys-PNCs.

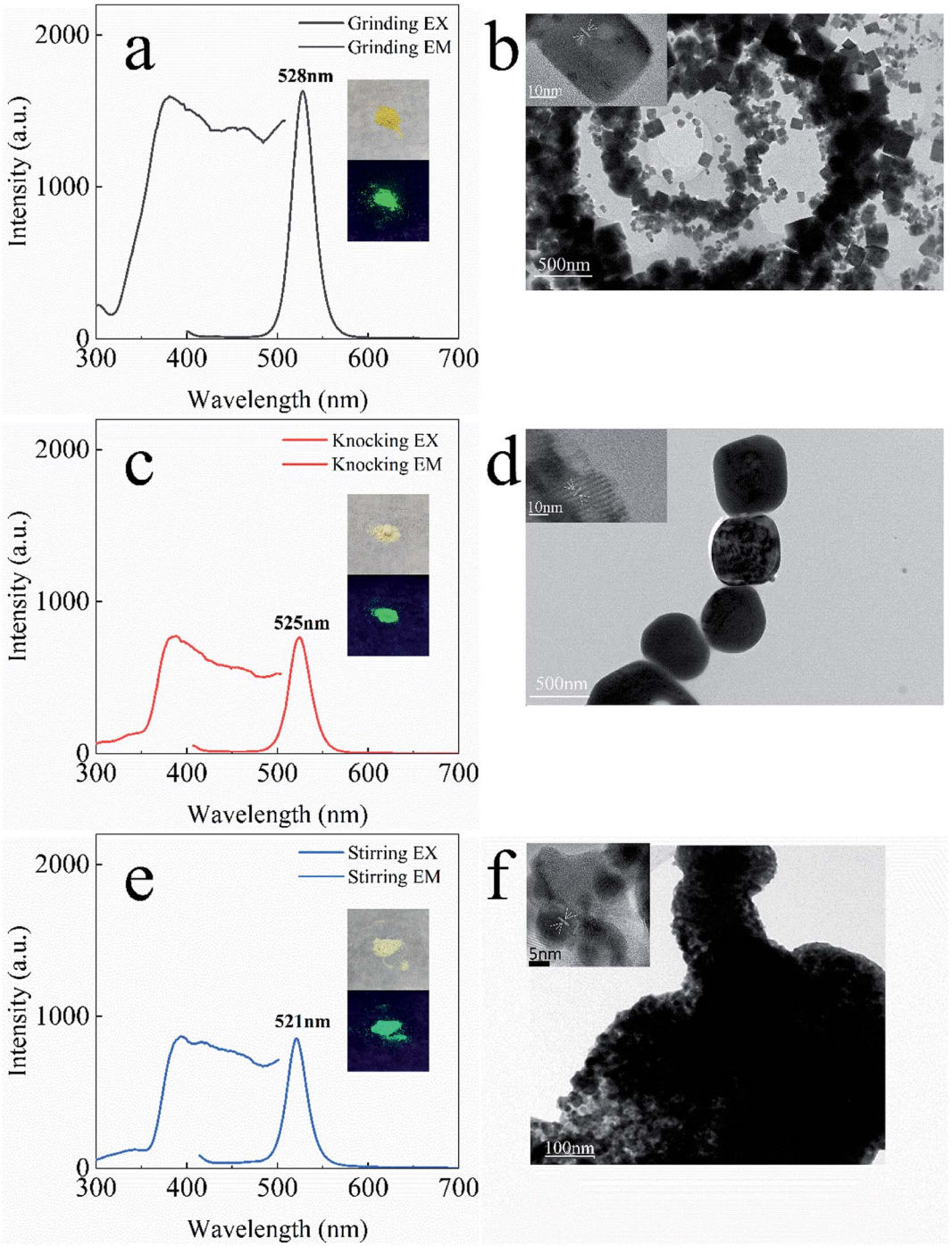

Fig. 2 Photoluminescence spectrum and corresponding TEM images of Lys-PNCs obtained by different solid-phase synthesis methods. The excitation wavelength in (a, c and e) is 380 nm, 387 nm and 394 nm, in which the illustrations are taken under daylight and 365 nm light. The TEM images of (b, d and f) correspond to the left.

3. Results and discussion

3.1 L-Lysine assisted solid-phase synthesis and characterization of the perovskite nanocrystals

Fig. 1 shows a schematic diagram of the L-lysine assisted solid-phase synthesis of PNCs. As the zwitterionic properties of amino acids, L-lysine would passivate Pb^{2+} and excess Br^{-} defects on the surface of perovskite particles that improve the effectiveness of ligand deactivation.[38] The possible role of L-lysine is roughly equivalent to the OLA (oleylamine) being protonated to OLA^{+} attached to the surface of the perovskite nanocrystal *via* the hydrogen bond between $-NH_3^{+}$ and Br^{-},[22,39–41] and the carboxyl group on OA (oleic acid) may bind to the nanocrystal surface as an ion pair with an amino group on the OLA.[39] Thereby surface defects are dynamically suppressed and thus the products emit strong luminescence. When the synthesis method is stirring, in which time the mechanical stress is small enough, the reactant can only obtain the energy of the reaction through the collision of its own molecules. At this time, only the product of structure 416 protected by L-lysine can be obtained. As the mechanical stress increases, the reaction is more likely to produce perovskite structure 113 that is not protected by L-lysine.

By using L-lysine as an assistant, the products obtained by three different solid-phase synthesis showed yellow-green (grinding), light-yellow (knocking), and green (stirring) color, and emitted strong green luminescence under ultraviolet light (Fig. 2a, c and e. We performed TEM and High-resolution TEM testing on the samples to observe the lattice of samples obtained by different methods (Fig. 2b, d and f). The sample obtained by grinding have obvious cubic nanocrystals under TEM (Fig. 2b). Some of the samples obtained by knocking turned into cubic nanocrystals, more in the form of nanospheres (Fig. 2d). Cube-shaped nanocrystals could not be obtained from the samples obtained by stirring (Fig. 2f), and all of them were nanospheres in agglomerated form. The morphology of the nanocrystals obtained from the three methods can be clearly seen from HR-TEM (the insets in Fig. 2b, d and f), which indicated that the nanocrystals were gradually grown from small nanospheres (5–8 nm, by stirring) to rectangular nanocrystals (50–200 nm, by knocking and grinding) in different ways of solid-synthesis. Therefore, based on the photoluminescence spectrum and TEM image, it can be inferred that different synthesis methods affect the shape and size of the nanocrystal, and its excitation and emission will also change accordingly. This change has a certain relationship with the production of 113 structure perovskite and its quantum size effect.[42–45]

The X-ray diffraction (XRD) was also used to verify the crystal structure of the products (Fig. 3). The XRD data of the products were aligned by indexing the databases of $CsPbBr_3$ (space group $Pm\bar{3}m$, PDF#75-0412) and Cs_4PbBr_6 (space group $R\bar{3}c$, PDF#73-2478). Among them, Grinding, which has the greatest mechanical stress, obtained a product with a 113 structure doped with a small amount of 416 structure perovskite. When the mechanical stress is slightly reduced and the collision of magnetons is used to provide reaction energy, the reaction

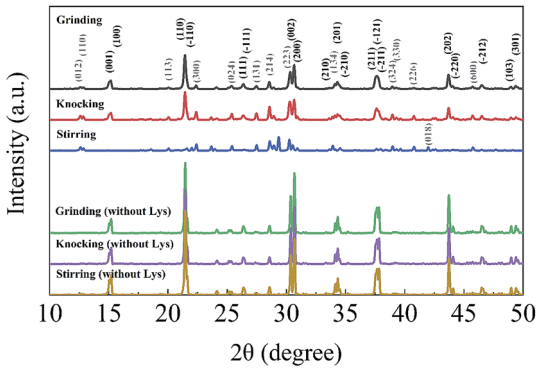

Fig. 3 XRD of Lys-PNCs obtained by different solid-phase synthesis methods, and XRD of the blank control samples without L-lysine.

cannot get more 113 structure perovskite. When the mechanical stress is weakened to only rely on the collision of the reactants themselves to provide reaction energy, the reaction can only get the product of the 416 structure. This difference indicates that the magnitude of the reaction force also affects the change in the optimal growth direction of the crystal plane of the raw material. The X-ray diffraction differences of the crystals also indicate that the luminescence of the nanocrystals synthesized with the assistance of L-lysine is the structural feature of different configurations of perovskites. In the blank sample without L-lysine, only the 113 structure perovskite can be obtained through the three methods. This phenomenon shows that the addition of L-lysine and the control of mechanical stress can make the perovskite product grow to the 416 structure of 0D perovskite first. With the increase of mechanical stress, L-lysine, which accounts for only 0.2 times of the Cs and Pb raw materials, can no longer prevent the growth of its product crystals, so that in the grinding sample, a product with a 113 structure perovskite as the main body is obtained.

To illustrate the reaction of L-lysine in cesium lead halide perovskite, X-ray photoelectron spectroscopy (XPS) was used to analyze the element changes of the products. The product synthesis by the method of stirring was chosen for studying because the product obtained by stirring has the weakest mixing force in the three solid-synthesis methods. At this time, the product was controlled by L-lysine as the main reason. As shown in Fig. 4, The Cs 3d signal (Fig. 4a) has similar binding energy to $CsPbBr_3$ quantum dots[46] and Cs_4PbBr_6 nanosheets.[47] The low energy shoulder of the Pb 4f (Fig. 4b) main peak indicates that the surface Pb ions are not reacted in the product except for the portion participating in the reaction.[46] At binding energies of 68.73 and 69.78 eV, the Br 3d (Fig. 4c) peak can be divided into two peaks, due to internal and surface Br ions, respectively.[46,48] The N 1s signal (Fig. 4d) can be attributed to two different amino groups on L-lysine.

The Fourier transform-infrared spectroscopy (FTIR) spectrum of L-lysine (Fig. 4e) has two bands at 2864 and 2934 cm^{-1}, respectively, which attributing to asymmetric and symmetric C–H_2 stretching. Both two bands were confirmed in the product. A carbonyl stretching band of carboxylic acid was observed at

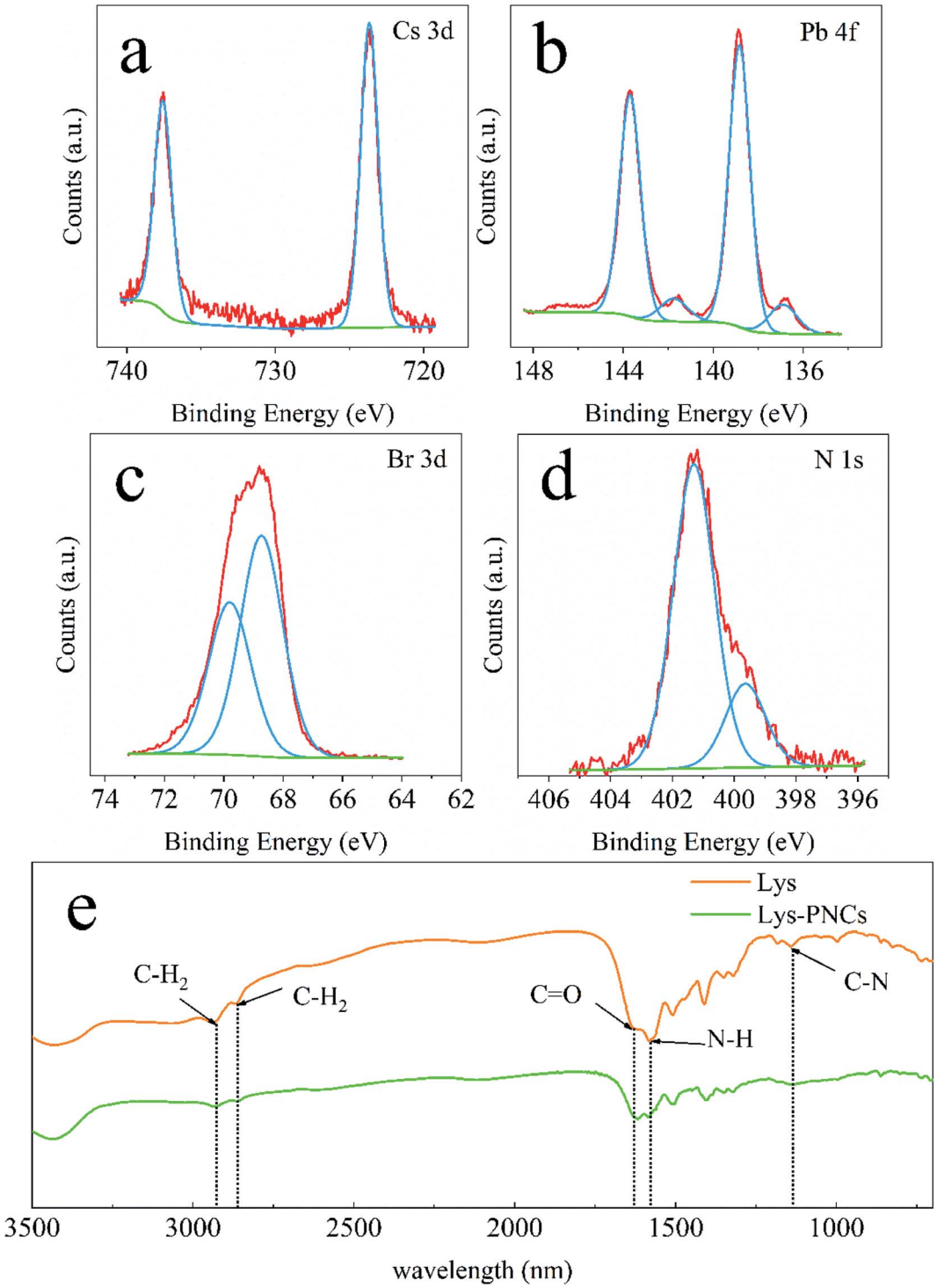

Fig. 4 Structural analysis of Lys-PNCs obtained by stirring. The XPS spectra of Lys-PNCs (a) Cs 3d, (b) Pb 4f, (c) Br 3d, (d) N 1s. (e) The Fourier transform-infrared spectroscopy (FTIR) spectrum of L-lysine and Lys-PNCs.

1617 cm^{-1}. Bands at 1582 and 1143 cm^{-1} were designated as N–H in-plane bends and C–N stretched amines, respectively. Furthermore, the peak position of Br 3d in XPS is shifted by about 1.0 eV relative to the high binding energy (BE) in other literatures,[46,47,49] indicating the effect of $-NH_3^+$ in L-lysine on the surface Br^- defect sites.[50] While the FTIR spectrum of the product appears in the characteristic peak of the L-lysine functional group, it has different degrees of attenuation and enhancement, especially the weakening of the C–N bond. Both above phenomena indicate that L-lysine is well involved in the reaction.

Considering L-lysine is a member of the amino acid, other amino acids were also selected to study the solid-phase synthesis of PNCs. Comparing with the blank sample, the results (ESI, Fig. S1†) indicated that although several amino acids can also assist the synthesis of luminescent PNCs, the effect of the amino acids is much weak than that of L-lysine. The results are in accord with the report that bifunctional ligands of peptide-like molecules containing both amino and carboxylic groups could effectively passivate cationic and anionic surface defect sites on the different types of PNCs surface.[50] The reason why L-lysine has outstanding effect better than other amino acid in solid-phase synthesis still needs more studies to uncover.

3.2 Comparison of the three solid-phase synthesis methods

The products synthesized by the three solid-phase methods have different emission wavelength positions (Fig. 2a, c and e) and different XRD spectra (Fig. 3). The result indicated that the synthesis force and the surface exposure during the mixing of the reactants in the solid phase reaction determine the formation of crystals. As we have known, the milling time is a prerequisite for the desired mechanochemical reaction which significantly depends on the initial particle size.[51] The lack of the rapid and direct synthesis of a perovskite product by a ball mill is attributed to a kinetic limitation associated with difficulties in developing a mill capable of providing highly energetic impacts that are critical to managing the

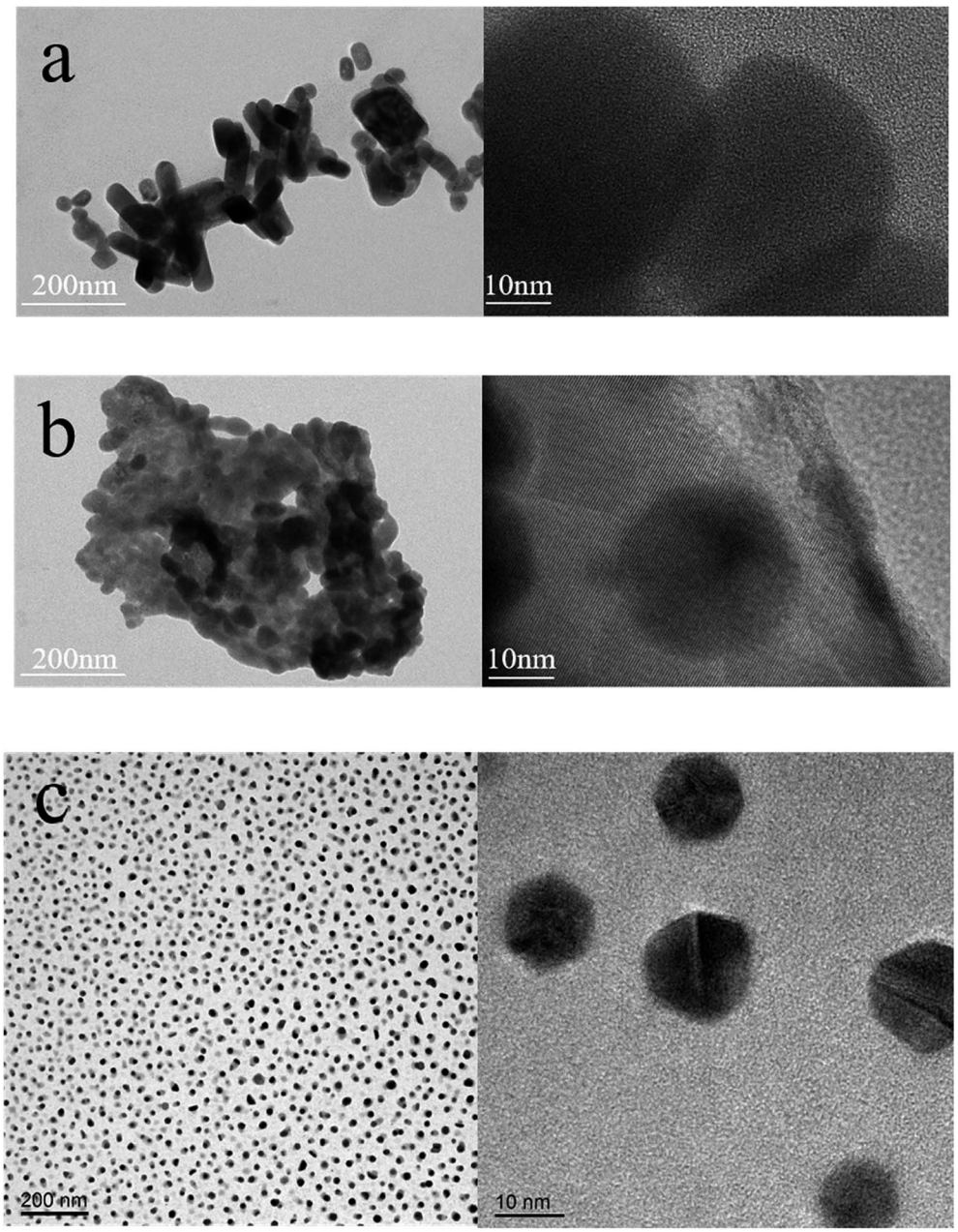

Fig. 5 TEM/HRTEM image of Lys-PNCs in water obtained by (a) grinding, (b) knocking, (c) stirring.

mechanochemical reaction and related yield. Theoretical modeling of kinematic equations describing the energy transfer of the ball to the powder in a planetary mill was well established by Burgio *et al.*[52] Given that the level of energy and number of impacts transferred to the reactant powders may be correlated with an intrinsic activation energy barrier of the reaction system, the higher activation energy level of a given reaction, the more energetic milling condition is needed to cause a reaction between starting materials mechanochemically.[53] A number of papers have described the morphological transformation process during the synthesis of perovskite by mechanochemical reaction.

Although the perovskite in the pure phase was not obtained by short grinding in this experiment (Fig. 3), the L-lysine-coated product has more excellent light-emitting performance (Fig. S1a†). This shows that L-lysine has a positive effect in quickly obtaining cesium lead perovskite with strong luminescence. Combining the results of the reaction, we found that three solid-state synthesis obtain perovskite crystal structures (Fig. 3b), which follow the mechanochemical synthesis rules outlined in the above-mentioned literature. The samples obtained by grinding not only have stronger luminescence performance and longer fluorescence lifetime, but also have the best light stability among the three. But also in the air (Fig. S4†), Knocking has the strongest stability. Stored at low temperature in the dark (Fig. S5†), the samples obtained by stirring can maintain the best long-term stability.

However, the luminescence intensity and the stability of the products can be directly related to the morphology uniformity of nanocrystals (Fig. 2 and S2, S3, S4, S5†). The stability of products with different structural tendencies under different conditions is also very different. It is a pity that we cannot combine the advantages of products with different mechanical stresses to get the best samples. Therefore, we tried to improve this problem in terms of raw materials.

3.3 Water assisted grinding synthesis of Lys-PNC

As the L-lysine is water soluble, it is worthy to study the role of water on the morphological structure and luminescence property of Lys-PNCs by solid-phase method. Thus, some water was added to the raw materials before synthesis. The properties of the nanocrystals obtained by three different methods are still very different after being sufficiently dispersed by water. As shown in the TEM images, cubic perovskite nanocrystals cannot be found in the product by grinding completely, which is consistent with the properties of perovskite itself (Fig. 5a). The mixed nanocrystals obtained by knocking were able to retain many crystal lattices after exposure to water, and small polygonal nanocrystals appeared (Fig. 5b). Large number of well dispersed small polygonal nanocrystals can be found in the sample of stirring (Fig. 5c). The changes of TEM images indicated that the nanocrystals obtained under weak forces can maintain good dispersibility and crystal structure in water.

We have achieved direct synthesis of Lys-PNCs in water by incasing the amount of L-lysine in solid-phase synthesis (Fig. 6). Taking the product obtained by grinding synthesis as an

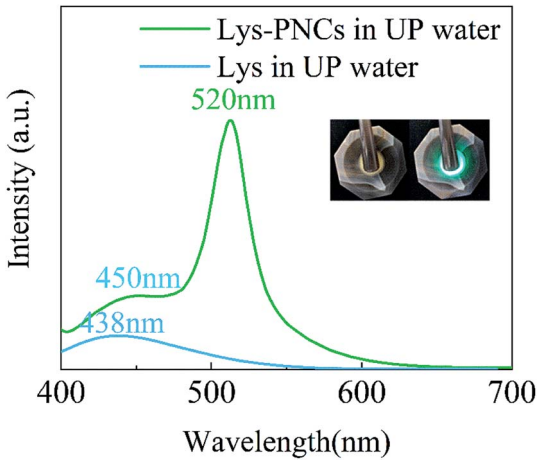

Fig. 6 Emission spectra of Lys-PNCs obtained by Water-assisted solid-phase synthesis. The illustrations are Lys-PNCs taken under daylight and 365 nm light.

example, after sufficient grinding, L-lysine, which participates in the reaction, has a much higher affinity for water than the perovskite, so it has a tendency to dissolve in water, but its decomposition is not suddenly. We give the picture after a brief water assisted grinding synthesis (the inset of Fig. 6). The color of the turbid liquid is not significantly different from the solid color. It can be seen that L-lysine has a certain protective effect on nanocrystal. The product has two emissions at 520 and 450 nm which are originated from the Lys-PNCs and the excess L-lysine, respectively (Fig. 6). Due to the trapped state or quantum size effect on the surface of PNCs passivated by L-lysine, the morphology of PNCs becomes complicated, so that the peak at 438 nm is shifted and enhanced.[38] In this reaction, the problem of excessive viscosity of solid powder in the solid-phase reaction was solved by adding water without affecting its strong luminescence. However, when we took the dry precipitate after washing several times for XRD, it was found that there was no crystal form of perovskite in the mixed powder (Fig. S6†). It shows that under the action of multiple centrifugal forces, the water dissolves into the complete L-lysine reaction. The surface of the perovskite lacks $-NH_2$ to compensate for the defects, and the structure becomes extremely unstable and eventually hydrolyzed.

However, due to the increase in the amount of L-lysine, products with green fluorescence emission cannot be obtained by stirring under the same reaction conditions after adding water. This experiment demonstrates that the use of excess L-lysine maintains the water stability of Lys-PNCs. As a ligand of Lys-PNCs, L-lysine has certain biological characteristics, which shows that Lys-PNCs has certain potential in analysis and detection. As a ligand of Lys-PNCs, L-lysine has certain biological characteristics, which shows that Lys-PNCs has certain potential in analysis and detection. In addition, because the synthesis process is extremely simple, we can directly participate in the reaction of the test substance, and use the luminous performance as a signal to judge the test substance. The water assisted synthesis method provides a way for detection in water.

4. Conclusions

In this work, a green solid-phase synthesis method without using organic solvents was successfully realized to synthesize luminescent PNCs in very short time. By comparing three solid-phase synthesis methods of grinding, knocking and stirring synthesis, we found the growth mode of perovskite in different reaction stages with the assistance of L-lysine. At the same time, in order to get this good performance and simplify the synthesis, L-lysine is crucial. Due to the characteristics of amino acids, Lys-PNCs has enhanced resistance to water, so that it can be solid-phase synthesized in water, which has the potential of biomass detection. The L-lysine assisted solid-phase synthesis methods proposed here would obtain more new perovskites by modifications and provided potential application of perovskite in many fields.

Conflicts of interest

There are no conflicts to declare.

Acknowledgements

This work was financially supported by the National Natural Science Foundation of China (No. 21565030), Program for Excellent Young Talents of Yunnan University and Foundation of National Demonstration Center for Experimental Chemistry and Chemical Engineering Education (Yunnan University).

References

1 P. Qin, S. Tanaka, S. Ito, N. Tetreault, K. Manabe, H. Nishino, M. K. Nazeeruddin and M. Grätzel, Inorganic hole conductor-based lead halide perovskite solar cells with 12.4% conversion efficiency, *Nat. Commun.*, 2014, **5**, 3834.

2 N. J. Jeon, J. H. Noh, W. S. Yang, Y. C. Kim, S. Ryu, J. Seo and S. I. Seok, Compositional engineering of perovskite materials for high-performance solar cells, *Nature*, 2015, **517**, 476.

3 P. Docampo, J. M. Ball, M. Darwich, G. E. Eperon and H. J. Snaith, Efficient organometal trihalide perovskite planar-heterojunction solar cells on flexible polymer substrates, *Nat. Commun.*, 2013, **4**, 2761.

4 H.-S. Kim, I. Mora-Sero, V. Gonzalez-Pedro, F. Fabregat-Santiago, E. J. Juarez-Perez, N.-G. Park and J. Bisquert, Mechanism of carrier accumulation in perovskite thin-absorber solar cells, *Nat. Commun.*, 2013, **4**, 2242.

5 S. D. Stranks, G. E. Eperon, G. Grancini, C. Menelaou, M. J. P. Alcocer, T. Leijtens, L. M. Herz, A. Petrozza and H. J. Snaith, Electron-Hole Diffusion Lengths Exceeding 1 Micrometer in an Organometal Trihalide Perovskite Absorber, *Science*, 2013, **342**(6156), 341.

6 A. Mei, X. Li, L. Liu, Z. Ku, T. Liu, Y. Rong, M. Xu, M. Hu, J. Chen, Y. Yang, M. Grätzel and H. Han, A hole-conductor–free, fully printable mesoscopic perovskite solar cell with high stability, *Science*, 2014, **345**(6194), 295.

7 J. A. Christians, R. C. M. Fung and P. V. Kamat, An Inorganic Hole Conductor for Organo-Lead Halide Perovskite Solar Cells. Improved Hole Conductivity with Copper Iodide, *J. Am. Chem. Soc.*, 2014, **136**(2), 758–764.

8 D. Liu, J. Yang and T. L. Kelly, Compact Layer Free Perovskite Solar Cells with 13.5% Efficiency, *J. Am. Chem. Soc.*, 2014, **136**(49), 17116–17122.

9 W. Nie, H. Tsai, R. Asadpour, J.-C. Blancon, A. J. Neukirch, G. Gupta, J. J. Crochet, M. Chhowalla, S. Tretiak, M. A. Alam, H.-L. Wang and A. D. Mohite, High-efficiency solution-processed perovskite solar cells with millimeter-scale grains, *Science*, 2015, **347**(6221), 522.

10 J. J. Choi, X. Yang, Z. M. Norman, S. J. L. Billinge and J. S. Owen, Structure of Methylammonium Lead Iodide Within Mesoporous Titanium Dioxide: Active Material in High-Performance Perovskite Solar Cells, *Nano Lett.*, 2014, **14**(1), 127–133.

11 H. Zhu, Y. Fu, F. Meng, X. Wu, Z. Gong, Q. Ding, M. V. Gustafsson, M. T. Trinh, S. Jin and X. Y. Zhu, Lead halide perovskite nanowire lasers with low lasing thresholds and high quality factors, *Nat. Mater.*, 2015, **14**(6), 636–642.

12 S. Yakunin, L. Protesescu, F. Krieg, M. I. Bodnarchuk, G. Nedelcu, M. Humer, G. De Luca, M. Fiebig, W. Heiss and M. V. Kovalenko, Low-threshold amplified spontaneous emission and lasing from colloidal nanocrystals of caesium lead halide perovskites, *Nat. Commun.*, 2015, **6**, 8056.

13 G. Xing, N. Mathews, S. S. Lim, N. Yantara, X. Liu, D. Sabba, M. Grätzel, S. Mhaisalkar and T. C. Sum, Low-temperature solution-processed wavelength-tunable perovskites for lasing, *Nat. Mater.*, 2014, **13**, 476.

14 Y. Wang, X. Li, J. Song, L. Xiao, H. Zeng and H. Sun, All-Inorganic Colloidal Perovskite Quantum Dots: A New Class of Lasing Materials with Favorable Characteristics, *Adv. Mater.*, 2015, **27**(44), 7101–7108.

15 Z.-K. Tan, R. S. Moghaddam, M. L. Lai, P. Docampo, R. Higler, F. Deschler, M. Price, A. Sadhanala, L. M. Pazos, D. Credgington, F. Hanusch, T. Bein, H. J. Snaith and R. H. Friend, Bright light-emitting diodes based on organometal halide perovskite, *Nat. Nanotechnol.*, 2014, **9**, 687.

16 L. Dou, Y. Yang, J. You, Z. Hong, W.-H. Chang, G. Li and Y. Yang, Solution-processed hybrid perovskite photodetectors with high detectivity, *Nat. Commun.*, 2014, **5**, 5404.

17 S. Yakunin, M. Sytnyk, D. Kriegner, S. Shrestha, M. Richter, G. J. Matt, H. Azimi, C. J. Brabec, J. Stangl, M. V. Kovalenko and W. Heiss, Detection of X-ray photons by solution-processed lead halide perovskites, *Nat. Photonics*, 2015, **9**, 444.

18 P. Ramasamy, D.-H. Lim, B. Kim, S.-H. Lee, M.-S. Lee and J.-S. Lee, All-inorganic cesium lead halide perovskite nanocrystals for photodetector applications, *Chem. Commun.*, 2016, **52**(10), 2067–2070.

19 L. Lv, Y. Xu, H. Fang, W. Luo, F. Xu, L. Liu, B. Wang, X. Zhang, D. Yang, W. Hu and A. Dong, Generalized colloidal synthesis of high-quality, two-dimensional cesium lead halide perovskite nanosheets and their

applications in photodetectors, *Nanoscale*, 2016, **8**(28), 13589–13596.

20 Y.-S. Chen, J. S. Manser and P. V. Kamat, All Solution-Processed Lead Halide Perovskite-BiVO4 Tandem Assembly for Photolytic Solar Fuels Production, *J. Am. Chem. Soc.*, 2015, **137**(2), 974–981.

21 C. K. Møller, Crystal Structure and Photoconductivity of Cæsium Plumbohalides, *Nature*, 1958, **182**(4647), 1436.

22 L. Protesescu, S. Yakunin, M. I. Bodnarchuk, F. Krieg, R. Caputo, C. H. Hendon, R. X. Yang, A. Walsh and M. V. Kovalenko, Nanocrystals of Cesium Lead Halide Perovskites (CsPbX3, X = Cl, Br, and I): Novel Optoelectronic Materials Showing Bright Emission with Wide Color Gamut, *Nano Lett.*, 2015, **15**(6), 3692–3696.

23 D. Zhang, S. W. Eaton, Y. Yu, L. Dou and P. Yang, Solution-Phase Synthesis of Cesium Lead Halide Perovskite Nanowires, *J. Am. Chem. Soc.*, 2015, **137**(29), 9230–9233.

24 S. Sun, D. Yuan, Y. Xu, A. Wang and Z. Deng, Ligand-Mediated Synthesis of Shape-Controlled Cesium Lead Halide Perovskite Nanocrystals via Reprecipitation Process at Room Temperature, *ACS Nano*, 2016, **10**(3), 3648–3657.

25 Y. Bekenstein, B. A. Koscher, S. W. Eaton, P. Yang and A. P. Alivisatos, Highly Luminescent Colloidal Nanoplates of Perovskite Cesium Lead Halide and Their Oriented Assemblies, *J. Am. Chem. Soc.*, 2015, **137**(51), 16008–16011.

26 Q. A. Akkerman, S. G. Motti, A. R. Srimath Kandada, E. Mosconi, V. D'Innocenzo, G. Bertoni, S. Marras, B. A. Kamino, L. Miranda, F. De Angelis, A. Petrozza, M. Prato and L. Manna, Solution Synthesis Approach to Colloidal Cesium Lead Halide Perovskite Nanoplatelets with Monolayer-Level Thickness Control, *J. Am. Chem. Soc.*, 2016, **138**(3), 1010–1016.

27 H. Huang, L. Polavarapu, J. A. Sichert, A. S. Susha, A. S. Urban and A. L. Rogach, Colloidal lead halide perovskite nanocrystals: synthesis, optical properties and applications, *NPG Asia Mater.*, 2016, **8**, e328.

28 A. Jancik Prochazkova, S. Demchyshyn, C. Yumusak, J. Másilko, O. Brüggemann, M. Weiter, M. Kaltenbrunner, N. S. Sariciftci, J. Krajcovic, Y. Salinas and A. Kovalenko, Proteinogenic Amino Acid Assisted Preparation of Highly Luminescent Hybrid Perovskite Nanoparticles, *ACS Appl. Nano Mater.*, 2019, **2**(7), 4267–4274.

29 J.-H. Jeon, Mechanochemical synthesis and mechanochemical activation-assisted synthesis of alkaline niobate-based lead-free piezoceramic powders, *Curr. Opin. Chem. Eng.*, 2014, **3**, 30–35.

30 Q. Zhang and F. Saito, A review on mechanochemical syntheses of functional materials, *Adv. Powder Technol.*, 2012, **23**(5), 523–531.

31 F. Palazon, Y. El Ajjouri and H. J. Bolink, Making by Grinding: Mechanochemistry Boosts the Development of Halide Perovskites and Other Multinary Metal Halides, *Adv. Energy Mater.*, 2019, 1902499.

32 T. Rojac, A. Benčan and M. Kosec, Mechanism and Role of Mechanochemical Activation in the Synthesis of (K,Na,Li)(Nb,Ta)O3 Ceramics, *J. Am. Ceram. Soc.*, 2010, **93**(6), 1619–1625.

33 R. Singh, P. K. Patro, A. R. Kulkarni and C. S. Harendranath, Synthesis of nano-crystalline potassium sodium niobate ceramic using mechanochemical activation, *Ceram. Int.*, 2014, **40**(7), 10641–10647.

34 D. Chen, J. Li, X. Chen, J. Chen and J. Zhong, Grinding Synthesis of APbX3 (A = MA, FA, Cs; X = Cl, Br, I) Perovskite Nanocrystals, *ACS Appl. Mater. Interfaces*, 2019, **11**(10), 10059–10067.

35 F. Palazon, Y. El Ajjouri, P. Sebastia-Luna, S. Lauciello, L. Manna and H. J. Bolink, Mechanochemical synthesis of inorganic halide perovskites: evolution of phase-purity, morphology, and photoluminescence, *J. Mater. Chem. C*, 2019, **7**(37), 11406–11410.

36 P. Pal, S. Saha, A. Banik, A. Sarkar and K. Biswas, All-Solid-State Mechanochemical Synthesis and Post-Synthetic Transformation of Inorganic Perovskite-type Halides, *Chem.–Eur. J.*, 2018, **24**(8), 1811–1815.

37 Z.-Y. Zhu, Q.-Q. Yang, L.-F. Gao, L. Zhang, A.-Y. Shi, C.-L. Sun, Q. Wang and H.-L. Zhang, Solvent-Free Mechanosynthesis of Composition-Tunable Cesium Lead Halide Perovskite Quantum Dots, *J. Phys. Chem. Lett.*, 2017, **8**(7), 1610–1614.

38 S. Wang, L. Zhou, F. Huang, Y. Xin, P. Jin, Q. Ma, Q. Pang, Y. Chen and J. Z. Zhang, Hybrid organic–inorganic lead bromide perovskite supercrystals self-assembled with l-cysteine and their good luminescence properties, *J. Mater. Chem. C*, 2018, **6**(41), 10994–11001.

39 J. De Roo, M. Ibáñez, P. Geiregat, G. Nedelcu, W. Walravens, J. Maes, J. C. Martins, I. Van Driessche, M. V. Kovalenko and Z. Hens, Highly Dynamic Ligand Binding and Light Absorption Coefficient of Cesium Lead Bromide Perovskite Nanocrystals, *ACS Nano*, 2016, **10**(2), 2071–2081.

40 D. Yang, X. Li and H. Zeng, Surface Chemistry of All Inorganic Halide Perovskite Nanocrystals: Passivation Mechanism and Stability, *Adv. Mater. Interfaces*, 2018, **5**(8), 1701662.

41 S. Sourisseau, N. Louvain, W. Bi, N. Mercier, D. Rondeau, F. Boucher, J.-Y. Buzaré and C. Legein, Reduced Band Gap Hybrid Perovskites Resulting from Combined Hydrogen and Halogen Bonding at the Organic−Inorganic Interface, *Chem. Mater.*, 2007, **19**(3), 600–607.

42 J. A. Sichert, Y. Tong, N. Mutz, M. Vollmer, S. Fischer, K. Z. Milowska, R. García Cortadella, B. Nickel, C. Cardenas-Daw, J. K. Stolarczyk, A. S. Urban and J. Feldmann, Quantum Size Effect in Organometal Halide Perovskite Nanoplatelets, *Nano Lett.*, 2015, **15**(10), 6521–6527.

43 J. Hou, S. Cao, Y. Wu, Z. Gao, F. Liang, Y. Sun, Z. Lin and L. Sun, Inorganic Colloidal Perovskite Quantum Dots for Robust Solar CO2 Reduction, *Chem.–Eur. J.*, 2017, **23**(40), 9481–9485.

44 Y.-H. Kim, C. Wolf, Y.-T. Kim, H. Cho, W. Kwon, S. Do, A. Sadhanala, C. G. Park, S.-W. Rhee, S. H. Im, R. H. Friend and T.-W. Lee, Highly Efficient Light-Emitting Diodes of Colloidal Metal–Halide Perovskite Nanocrystals beyond Quantum Size, *ACS Nano*, 2017, **11**(7), 6586–6593.

45 H.-C. Wang, S.-Y. Lin, A.-C. Tang, B. P. Singh, H.-C. Tong, C.-Y. Chen, Y.-C. Lee, T.-L. Tsai and R.-S. Liu, Mesoporous Silica Particles Integrated with All-Inorganic CsPbBr3 Perovskite Quantum-Dot Nanocomposites (MP-PQDs) with High Stability and Wide Color Gamut Used for Backlight Display, *Angew. Chem., Int. Ed.*, 2016, **55**(28), 7924–7929.

46 X. Li, Y. Wu, S. Zhang, B. Cai, Y. Gu, J. Song and H. Zeng, CsPbX3 Quantum Dots for Lighting and Displays: Room-Temperature Synthesis, Photoluminescence Superiorities, Underlying Origins and White Light-Emitting Diodes, *Adv. Funct. Mater.*, 2016, **26**(15), 2435–2445.

47 P. Uthirakumar, M. Devendiran, J. H. Park and I.-H. Lee, Reprecipitation induced isolation of ligand-free Cs4PbBr6 nanodisks as a green emissive UV light filter, *Prog. Org. Coat.*, 2019, **132**, 1–8.

48 F. Zhang, H. Zhong, C. Chen, X.-G. Wu, H. Xiangmin, H. Huang, J. Han, B. Zou and Y. Dong, Brightly Luminescent and Color-Tunable Colloidal CH 3 NH 3 PbX 3 (X = Br, I, Cl) Quantum Dots: Potential Alternatives for Display Technology, *ACS Nano*, 2015, **9**(4), 4533–4542.

49 X. Chen, F. Zhang, Y. Ge, L. Shi, S. Huang, J. Tang, Z. Lv, L. Zhang, B. Zou and H. Zhong, Centimeter-Sized Cs4PbBr6 Crystals with Embedded CsPbBr3 Nanocrystals Showing Superior Photoluminescence: Nonstoichiometry Induced Transformation and Light-Emitting Applications, *Adv. Funct. Mater.*, 2018, **28**(16), 1706567.

50 B. Luo, S. B. Naghadeh, A. L. Allen, X. Li and J. Z. Zhang, Peptide-Passivated Lead Halide Perovskite Nanocrystals Based on Synergistic Effect between Amino and Carboxylic Functional Groups, *Adv. Funct. Mater.*, 2017, **27**(6), 1604018.

51 A. Shrivastava, S. Sakthivel, B. Pitchumani and A. Rathore, A statistical approach for estimation of significant variables in wet attrition milling, *Powder Technol.*, 2011, **211**(1), 46–53.

52 N. Burgio, A. Iasonna, M. Magini, S. Martelli and F. Padella, Mechanical alloying of the Fe– Zr system. Correlation between input energy and end products, *Il nuovo cimento D*, 1991, **13**(4), 459–476.

53 G.-J. Lee, E.-K. Park, S.-A. Yang, J.-J. Park, S.-D. Bu and M.-K. Lee, Rapid and direct synthesis of complex perovskite oxides through a highly energetic planetary milling, *Sci. Rep.*, 2017, **7**, 46241.